Tunable Localized Plasmon Transducers Prepared by Thermal Dewetting of Percolated Evaporated Gold Films

7 AUTHORS, INCLUDING:

Alexander B Tesler
Harvard University
14 PUBLICATIONS **316** CITATIONS

SEE PROFILE

Tanya Karakouz
Medinol Ltd.
13 PUBLICATIONS **345** CITATIONS

SEE PROFILE

Gilad Haran
Weizmann Institute of Science
85 PUBLICATIONS **4,039** CITATIONS

SEE PROFILE

Alexander Vaskevich
Weizmann Institute of Science
**163** PUBLICATIONS **2,257** CITATIONS

SEE PROFILE

Tunable Localized Plasmon Transducers Prepared by Thermal Dewetting of Percolated Evaporated Gold Films

Alexander B. Tesler,[†] Lev Chuntonov,[‡] Tanya Karakouz,[†] Tatyana A. Bendikov,[§] Gilad Haran,[‡] Alexander Vaskevich,*,[†] and Israel Rubinstein*,[†]

[†]Deptartment of Materials and Interfaces, [‡]Deptartment of Chemical Physics, and [§]Deptartment of Chemical Research Support, Weizmann Institute of Science, Rehovot 76100, Israel

S *Supporting Information*

ABSTRACT: Gold island films displaying localized plasmon properties were prepared by evaporation of just-percolated Au films onto glass substrates followed by annealing at ≥550 °C. Annealing induces depercolation and formation of large, single-crystalline, well-separated islands, partially embedded in the glass. Two dewetting mechanisms were identified, depending on the initial film morphology. The variability of island sizes and shapes provides effective means of tuning the position of the localized surface plasmon resonance (LSPR) band in a wide wavelength range. With an increase in the Au nominal thickness a transition occurs from transducers dominated by absorbance to ones dominated by scattering. Numerical simulations taking into account the shape and size distribution in actual island samples are in agreement with the experimental spectra. Refractive index sensitivity (RIS) measurements at a constant wavelength or at a constant extinction, tailored to the specific transducer, provide superior sensitivity to refractive index change, up to ca. 600 nm RIU^{-1} in wavelength shift.
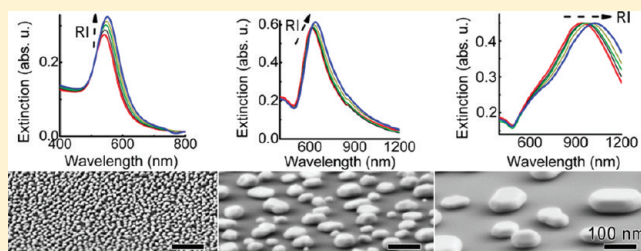
INTRODUCTION

Metal (e.g., gold, silver, copper, etc.) nanostructures exhibit special optical properties deriving from excitation of localized surface plasmon (SP) polaritons by electromagnetic radiation in the UV−vis−NIR spectral range. These special properties are expressed as strong light scattering, the appearance of intense SP absorption bands, and enhancement of local electromagnetic fields near the metal surface.[1] The sensitivity of SP extinction bands to the dielectric properties of the medium has been studied extensively as the basis for potential application in chemical and biological sensing.[2−15]

Tuning of the SP band wavelength is important with respect to various applications. Examples include photothermal therapy, where tuning of the SP absorbance to the NIR region is essential for providing better light penetration through the human tissue,[16] and plasmon-enhanced luminescence, where overlap between the surface plasmon band and the chromophore optical transition determines the enhancement.[17,18] In sensing applications it has been shown theoretically[5,19] and experimentally[3] that the refractive index sensitivity (RIS) of localized surface plasmon resonance (LSPR) transducers is directly correlated with the SP band wavelength, i.e., the RIS increases as the band is red shifted. The SP band can be tuned by various means.[20−22] A prominent example is rod-like metal nanostructures displaying transverse and longitudinal SP bands, where the wavelength of the latter can be tuned over much of the vis−NIR spectral region by changing the rod aspect ratio.[23−25] Use of multimetal (e.g., Au and Ag) nanoparticle (NP) systems also allows tuning of the LSPR extinction.[26−28]

Tunable SP bands of nanoparticulate noble metal films have been obtained by various means. Lithographic methods, either e-beam or colloidal lithography,[29−32] provide good control over the particle shape, dimensions, and array design, allowing efficient tuning of the SP band. However, these methods are not easily scalable for actual applications. A relatively simple approach is based on random ensembles of thermally evaporated metal nanoislands.[33−39] In such systems the evaporation conditions, e.g., the nominal thickness of the deposited metal, the evaporation rate,[40] and the substrate temperature, influence the position and shape of the SP band.[35,38,41,42] The method is convenient and scalable; however, the attainable spectral window of the SP band is rather limited, typically 450−600 nm for Ag island films[38] and 560−700 nm for Au island films.[37] SP tuning in a wider wavelength range requires special means, such as evaporation on a heated substrate,[35,43] multistep/multimetal evaporation,[33] or control of the refractive index (RI) of the substrate.[44,45] Hence, evaporation of a 40-nm-thick interlayer of ITO, ZrO_2, TiO_2, or Al_2O_3 on a quartz substrate enabled tuning of the SP of Ag island films from 500 to 950 nm.[46]

Preparation of metal (e.g., Au) island films by evaporation in high vacuum is frequently combined with postdeposition thermal treatments. Annealing of metal island films promotes island coarsening and an increase of the interparticle separation,

resulting in blue shift and sharpening of the SP band.[3,42,47] At the same time the annealing substantially reduces the SP tuning window. For thermally evaporated Au films on various dielectric substrates, the SP band wavelength varies from ca. 540 to ca. 700 nm in unannealed films of varied nominal thicknesses,[41,42] similar to the results of Norrman et al.,[37] while after annealing at 200—250 °C the SP wavelengths window shrinks to 530—590 nm.[41,42,48]

Studies concerning formation of island structure upon annealing of metal films of thicknesses in the vicinity of the percolation threshold are scarce compared to the large number of works devoted to annealing of island films or thick, fully percolated films.[42,49—52] Formation of well-defined island structures during annealing of near- and just-percolated Au films with nominal thicknesses of 7.5—15 nm was observed for Au films evaporated on mica,[47] quartz,[41] as well as bare[3] and silanized[42] glass. Island films were obtained by annealing at 435—500 °C of just-percolated Au films on ITO.[39,53] Annealing of just-percolated Ag and Cu films was also reported.[54,55] Just-percolated Ag films, 14—16 nm (nominal thickness), transformed to island films upon annealing.[54,56] The absence of a SP peak in as-deposited, 16 nm films suggested a percolated structure, which was transformed to islands after annealing at 600 K.[56] Annealing of near-percolated, 14 nm Ag films at 120—350 °C resulted in a blue shift of the SP band, from 700 to 450 nm, allowing tuning in a relatively large wavelength window.[54]

Substrates for metal-enhanced fluorescence were prepared by annealing of percolated, 15 nm Ag films,[57] while similar observations were reported, without detailed morphological characterization, for thermally depercolated Au films.[58] Near-percolated Ag films on passivated Si were used as substrates for SEIRA;[59] formation of the island film decreased the signal enhancement compare to the semicontinuous structure.

The present study concerns transformation of the morphology of just-percolated Au films containing a substantial number of voids during high-temperature annealing. It has been reported that dewetting of fully percolated films starts with formation of grooves[50,60—62] which become deeper due to capillary instability, eventually reaching the substrate. Depercolation and formation of individual islands proceeds via a continuous structure containing large, micrometer-scale areas of uncovered substrate.[49,63]

Our recent work on high-temperature annealing of Au island films vapor deposited on borosilicate glass slides showed that annealing at temperatures close to the glass transition temperature of the substrate (T_g = 557 °C) resulted in rapid change of the island film morphology as well as slow gradual embedding of the islands in the glass, thereby stabilizing the film morphology and optical response.[3,64] Annealing at high temperatures enhances not only the surface diffusion but also the recrystallization rate, allowing formation of ensembles of well-separated islands from relatively thick percolated Au films.

In the present work high-temperature annealing of evaporated Au films of variable nominal thicknesses (2—16 nm) was exploited for tuning the SP band in a wide wavelength range. Use of a range of Au nominal thicknesses (from island to just-percolated as-evaporated films) as substrates for subsequent high-temperature annealing enabled substantial extension of the SP tuning window (after annealing) from ca. 520 to ca. 900 nm. It is shown that dewetting of just-percolated films with substantial density of surface voids may follow different scenarios. Subject to the relative rate of recrystallization and dewetting, two types of dewetting mechanisms were identified: Dewetting of just-percolated films

thicker than a critical value (13 nm under the present conditions) results in formation of unique structures comprising large, submicrometer-size islands, which is morphologically different from that produced by annealing of initially discontinuous films. The measured RIS (for wavelength shift) of transducers prepared from Au films thicker than the critical thickness exhibits unusually large values, which correlate with the SP band wavelength.

The relatively large dimensions of the Au islands studied in the present work suggest that scattering can be a major component of the total extinction. Therefore, the optical properties of the island films are characterized here in both transmittance and reflectance modes[1,65—67] to analyze the relative contribution of the scattering and absorption components as a function of average Au island size, determined by the nominal evaporated thickness.

Development of the optical properties with an increase in the average island size is modeled using discrete dipole approximation (DDA) numerical simulations.[68—70] The influence of island shape and size distribution in the films is taken into account by using the actual experimental distributions. The calculated extinction spectra are in good agreement with the experimental results, demonstrating the possibility of effective theoretical analysis of the optical properties of random island films.

■ EXPERIMENTAL METHODS

Materials. Methanol (BioLab, AR, Israel), ethanol (Merck, AR), heptane (99% Sigma), propylene carbonate (Burdick & Jackson Laboratories, USA), toluene (Gadot, Israel), H_2O_2 (30% Frutarom, Israel), sulfuric acid (95—98%, Gadot, Israel), and gold (99.99%, Holland-Moran, Israel) were used as received. Rinsing of samples with water included sequentially washing in deionized and triply distilled water. The inert gas used was household nitrogen (from liquid N_2).

Substrate Preparation. Microscope cover glass slides (No. 3, Menzel-Gläser, Germany) cut to 22 × 9 mm were used as substrates for all Au films. The glass surface was cleaned from organic contaminants by immersion in freshly prepared piranha solution (1:3 H_2O_2, 30%:H_2SO_4, 95—98%) for 1 h followed by extensive rinsing with water and three times with ethanol in an ultrasonic bath (Cole-Parmer 8890), 5 min each. The cleaned glass substrates were stored in ethanol until use. Before Au deposition the slides were dried under a nitrogen stream.

Preparation of Au Films. Cleaned and dried glass substrates were mounted in a cryo-HV evaporator (Key High Vacuum) equipped with a Maxtek TM-100 thickness monitor. Homogeneous Au deposition was obtained by moderate rotation of the substrate plate. Au was resistively evaporated from a tungsten boat at $1—3 \times 10^{-6}$ Torr at a deposition rate of 0.005—0.01 nm s^{-1} (determined by measuring the evaporation time of 0.1 nm Au using a stopwatch). The samples were placed in a Kimax Petri dish and annealed in a Ney Vulcan 3—550 oven. In the case of short annealing (100 and 300 s) the samples were inserted into the preheated (to 550 °C) oven and removed after a predetermined time. The temperature was measured by means of a thermocouple contacting the inner part of the Petri dish bottom. Prolonged annealing was performed by inserting the samples into the oven, heating at a rate of 5 °C min^{-1}, holding the temperature at 550 °C for 10 h, and cooling to room temperature by natural convection in the oven. The morphology of the glass substrate after prolonged high-temperature annealing was studied by dissolution of the Au film in aqua regia.[64]
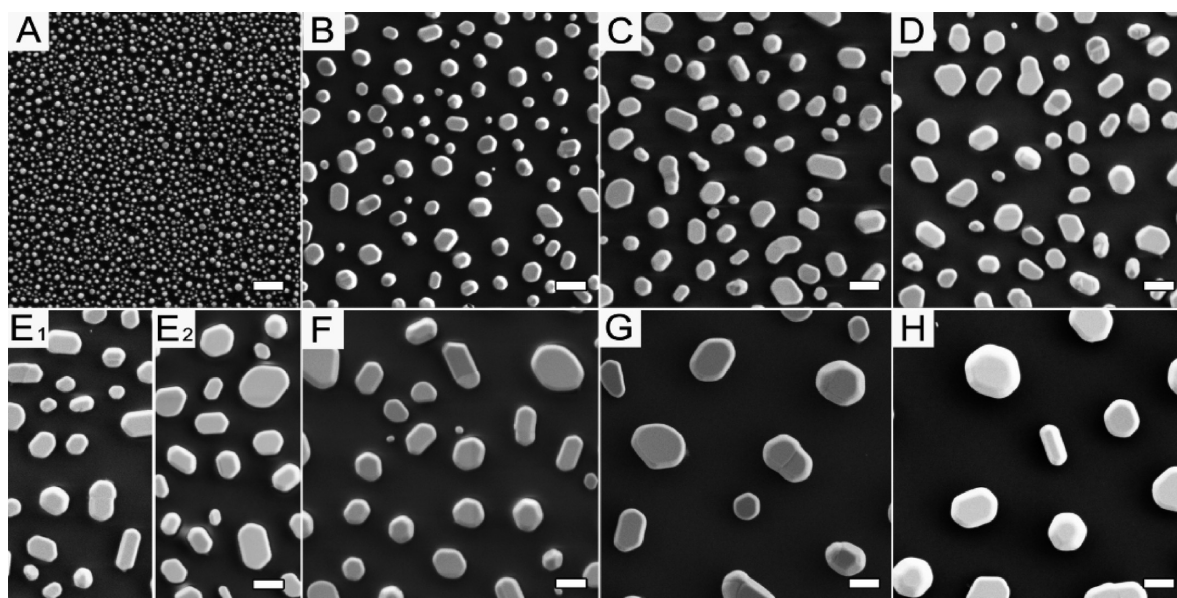
Figure 1. HRSEM images of Au films evaporated on glass substrates and annealed 10 h at 550 °C. Nominal thicknesses (in nm): (A) 5, (B) 10, (C) 11, (D) 12, (E_1 and E_2) 13, (F) 14, (G) 15, (H) 16. Scale bars: 200 nm.

High-Resolution Scanning Electron Microscopy (HRSEM). Scanning electron microscopy was performed using an ULTRA 55 FEG ZEISS microscope with a high-efficiency in-lens SE detector and an Everhart-Thornley secondary electron (SE) detector. Measurements were carried out at an applied voltage of 2 kV and a working distance of 3 mm. Glass substrates after dissolution of Au in aqua regia were coated with a 3 nm Cr overlayer prior to imaging to prevent charging.

Atomic Force Microscopy (AFM). Measurements were carried out in air at room temperature (22—23 °C) using a Molecular Imaging (MI) PicoScan instrument operating in the acoustic AC mode. The cantilevers used were NSC36 series of ultrasharp silicon (μMasch, Estonia) with a resonant frequency of 75—150 kHz and an average radius of $\leq$10 nm.

UV—Vis Spectroscopy. Transmission spectra of Au films before and after annealing were taken with a Varian CARY 50 UV/vis/NIR spectrophotometer. Combined measurements of transmission and total reflection were carried out with a Jasco V570 UV/vis/NIR dual-beam spectrophotometer equipped with an integration sphere attachment model ISV-469, providing a spectral window in the range 450—830 nm. Spectra were measured using a special slide holder that ensures reproducible positioning of the sample. The spectrum of air was taken as baseline for transmission measurements, while Spectrolon served as the reflection standard.

Refractive Index Sensitivity (RIS) Measurements. Transmission spectra were obtained with a Jasco V570 UV/vis/NIR dual-beam spectrophotometer. Au island samples were inserted into a 1 cm path quartz cuvette with an optical window of 170—2700 nm, while a matched cuvette with a bare glass slide immersed in the same solvent served as a reference. The slides were stabilized by dipping in ethanol and drying under a nitrogen stream several times until the spectrum remained unchanged and then measured in a given solvent. Usually the spectra remained constant after the first immersion. The solvents used were methanol (n = 1.329), ethanol (n = 1.362), heptane (n = 1.388), propylene carbonate (n = 1.421), and toluene (n = 1.496).

Table 1. Average Values and Standard Deviations of Morphological Parameters of Au Island Films Evaporated on Glass and Annealed 10 h at 550 °C[a]

nominal film thickness (nm)	major axis (nm)	aspect ratio (AR)	distance between center of mass[b] (nm)
5	23 ± 9	1.12 ± 0.12	36 ± 5
10	132 ± 44	1.24 ± 0.23	214 ± 4
11	173 ± 60	1.31 ± 0.26	264 ± 5
12	189 ± 71	1.33 ± 0.27	268 ± 5
13 Type I	243 ± 93	1.37 ± 0.34	368 ± 6
13 Type II	348 ± 114	1.43 ± 0.36	575 ± 10
14	237 ± 84	1.35 ± 0.30	403 ± 10
15	328 ± 117	1.42 ± 0.41	456 ± 16
16	340 ± 107	1.37 ± 0.27	640 ± 94

[a] Calculated from HRSEM images using ImageJ software. [b] Distance between centers of mass positions of four nearest neighbor particles.

The RI of the solvents was determined using an Abbe refractometer. The stability of the optical response was tested by carrying out the measurements sequentially in solvents with ascending and descending RI values, showing complete reproducibility, as reported previously.[3]

RESULTS AND DISCUSSION

Gold Island Films on Glass: Morphology and LSPR Spectroscopy. The morphology of thin Au films evaporated on glass and annealed 10 h at 550 °C was studied by high-resolution scanning electron microscopy (HRSEM) imaging (Figure 1). Films below a nominal thickness of ca. 10 nm (the nominal thickness, or mass thickness, is the thickness of a continuous, homogeneous film having the same Au mass) are initially discontinuous[3] (Figure S1, Supporting Information), whereas the as-evaporated 10—16 nm films are percolated[3,64,71] (Figure S2, Supporting Information). Annealing of the percolated 10—16 nm films at 550 °C results in formation of

24644

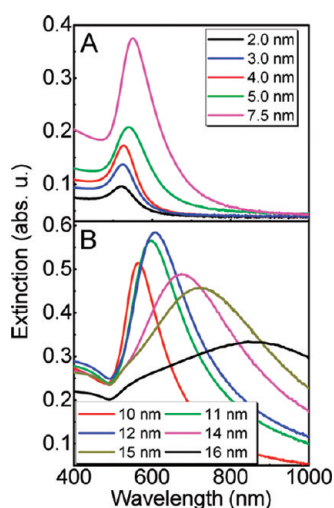dx.doi.org/10.1021/jp209114j |*J. Phys. Chem. C* 2011, 115, 24642–24652

Figure 2. Transmission UV−vis spectra of initially discontinuous (A) and initially percolated (B) Au films evaporated on glass substrates and annealed 10 h at 550 °C, measured in air. Nominal film thicknesses are indicated.
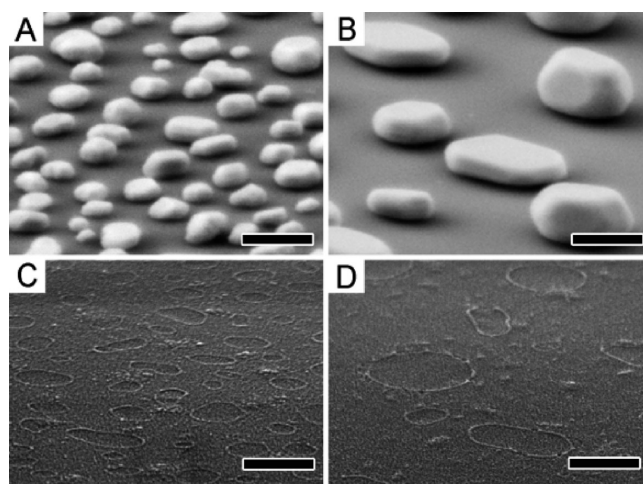

Figure 3. HRSEM images (projection view, tilted 70°) of (A) 10 and (B) 15 nm (nominal thicknesses) Au island films, evaporated on glass substrates and annealed 10 h at 550 °C. (C and D) Glass substrate after dissolution in aqua regia of the Au islands in A and B, respectively. Scale bars: 200 nm.

islands with scalable dimensions (Figure 1). Films produced from initially percolated Au layers (Figure 1B−H) present large, faceted islands with flat top surfaces. The average island diameter, island aspect ratio, and interparticle distance show a general tendency to increase as the Au nominal thickness becomes larger (Table 1), while the fraction of the area covered by islands and the number of particles per unit area decrease (Figure 1). Note that island films produced by annealing of 13 nm Au films form two families of islands (Figure $1E_1$ and $1E_2$ and Table 1 type I/II, respectively); this phenomenon is discussed later.

Transmission UV−vis spectra of initially discontinuous (2−7.5 nm, Figure 2A) and initially percolated (10−16 nm, Figure 2B) Au island films, prepared by evaporation on glass and annealing 10 h at 550 °C, are presented in Figure 2. The SP band of the 2−7.5 nm films shows a substantial intensity increase and a moderate red shift, from 520 to 560 nm, with increasing nominal thickness (Figure 2A). The thicker, initially percolated films (10−16 nm) show an intensity increase followed by a gradual decrease and a large red shift from 560 to 900 nm with increasing nominal thickness (Figure 2B). Hence, high-temperature annealing of discontinuous and just-percolated Au films enables tuning of the SP band in a range of ca. 400 nm.

Figure 3A and 3B presents 3D tilted-view HRSEM images of annealed 10 and 15 nm island films (Figure 1B and 1G), showing faceted, mostly single-crystalline islands with the (111) planes parallel to the substrate surface,[3] the latter confirmed by selected-area electron diffraction.[72] HRSEM (Figure 3C and 3D) and AFM (Figure S4, Supporting Information) imaging of similar island films after dissolution of the Au islands in aqua regia reveal depressions in the glass encircled by a glass rim, indicating partial embedding of the Au islands in the glass during the long high-temperature annealing, as previously reported.[3,64,71]

Depercolation of Just-Percolated Au Films. We have previously shown that the major morphological changes in Au island films annealed at high temperatures occur in the first few minutes; thereafter, the main process is slow embedding in the glass substrate, driven by capillary wetting in the vicinity of the glass transition temperature of the borosilicate glass (T_g = 557 °C).[64,71] In the present work the early stages of annealing,
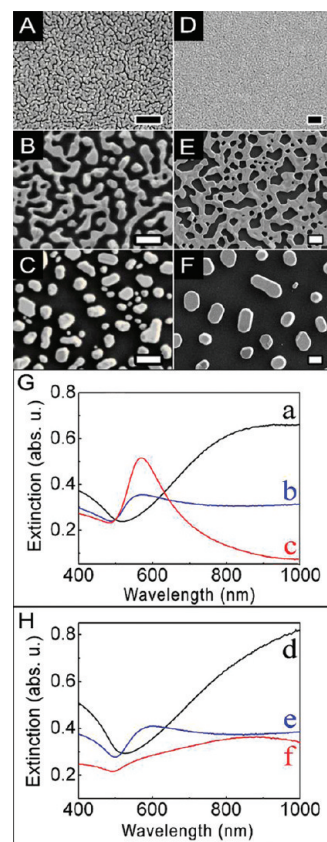
Figure 4. HRSEM images (A−F) and transmission UV−vis spectra (G, H) of 10 (A, B, C, G) and 15 nm (D, E, F, H) Au films evaporated on glass substrates and annealed at temperatures close to 550 °C (see Figure S3, Supporting Information). (A, a, D, d) As evaporated. Annealing times: (B, b) 100, (E, e) 140, and (C, c and F, f) 300 s. Scale bars: 200 nm.

encompassing the major morphological transformation, were studied for a series of just-percolated 10 and 15 nm Au films evaporated on glass. Figure 4 shows HRSEM images and corresponding

24645

dx.doi.org/10.1021/jp209114j |*J. Phys. Chem. C* 2011, 115, 24642–24652

Table 2. Average Values and Standard Deviations of Spectral Parameters of Au Island Films Evaporated on Glass and Annealed 10 h at 550 °C[a]

nominal film thickness (nm)	mean plasmon wavelength (nm)	mean extinction intensity (abs.u.)	mean fwhm (nm)[b]	figure of merit (FOM)[c]
5	524 ± 0.1	0.194 ± 0.003	59 ± 0.2	1.46
10	563 ± 3.5	0.503 ± 0.010	95 ± 4.2	1.65
11	595 ± 4.2	0.569 ± 0.005	137 ± 15.2	1.57
12	604 ± 4.3	0.585 ± 0.006	149 ± 4.8	1.18
13 type I	662 ± 17.0	0.514 ± 0.020	218 ± 10.4	1.37
13 type II	762 ± 21.0	0.379 ± 0.020	-	-
14	674 ± 12.7	0.489 ± 0.020	-	1.62
15	717 ± 18.9	0.458 ± 0.020	-	1.85
16	885 ± 47.8	0.325 ± 0.030	-	-

[a] Measurements carried out in air. [b] Dashes represent values which could not be determined. [c] FOM is defined as m_λ^{max}/fwhm.

spectra depicting critical stages of the film depercolation. The samples in Figure 4 were inserted into the preheated oven, and the slide temperature was measured using a digital thermometer. Due to the slow heating rate, at short annealing times the sample temperatures were somewhat lower than the oven set point of 550 °C (Figure S3, Supporting Information). However, similar experiments carried out at lower set-point temperatures (450 and 350 °C) showed slower kinetics but the same morphology evolution as in Figure 4. Note that the annealing temperature was close to $0.5 \times T_m$ ($T_m = 1337.6$ K is the melting temperature of bulk Au), implying facile recrystallization.[73]

The morphological transformation of the 10 nm Au film (Figure 4A) during short annealing at 550 °C follows a scenario where voids in the as-evaporated film progressively widen during the annealing, leading to formation of an ensemble of rather inhomogeneous features (Figure 4B). The film at this stage presents mostly complex, liquid-like shapes with a small fraction of symmetrical ellipsoid-like features. The corresponding transmission spectrum (Figure 4G, trace b) exhibits a superposition of the spectrum of large, ill-defined features (red tail) and an SP band at ca. 575 nm, the latter representing the already formed Au islands as well as the transverse SP of the elongated odd structures. Further annealing leads to completion of the dewetting and recrystallization of the irregularly shaped Au islands. The resulting ensemble of faceted islands displays a well-defined SP band at ca. 580 nm (Figure 4C and 4G, trace c).

Figure 4D—F presents the thermal dewetting at 550 °C of a thicker (15 nm) film (Figure 4H, trace d), showing a markedly different mechanism. Fast recrystallization of Au grains leads to formation of a continuous Au structure with a random ensemble of faceted holes, tens to hundreds of nanometers in diameter (Figure 4E). This structure supports excitation of localized SPs,[74] as seen in the corresponding transmission spectrum, exhibiting an SP band at 570 nm (Figure 4H, trace e). Continued annealing induces opening of boundaries between Au grains, leading to formation of large, single-crystalline Au islands with flat top surfaces (Figure 4F). The size, shape, and height distribution of these Au islands are broader than those of the annealed 10 nm island film, as seen in the data reported in Table 1; a detailed analysis is given elsewhere.[72] The SP extinction exhibits a complex structure with a shoulder around 550 nm and a broad main band in the near-IR region (Figure 4H, trace f).

The different thermal depercolation mechanisms observed for the 10 and 15 nm Au films are attributed to the different depth profile of voids in the as-evaporated (unannealed) films. While in thinner, just-percolated unannealed films the voids protrude through the Au film to the glass substrate, in thicker percolated films the voids do not reach the glass substrate. This difference in the initial morphology determines the depercolation pathway, as demonstrated and discussed elsewhere.[72] The two types of films are denoted type I and type II, respectively.

As noted above, the island film morphology reached after ca. 300 s of annealing at 550 °C remains essentially unchanged during further long annealing (10 h at 550 °C), with the main process being slow island embedding in the glass and formation of a glass rim around the islands.[3,64,71]

The spectral data compiled in Table 2 represent several batches (20 slides each) measured after annealing. The impressive range of tunable SP wavelength achieved with such films spans ca. 360 nm. Also evident in Table 2 is the trend in data scatter: While the standard deviation for annealed type I films is notably small, as reported previously,[3,75] annealed type II films show substantial scatter in the SP position, increasing with the film nominal thickness (Figure S5, Supporting Information). The mechanistic reasons underlying the increased variability in the dewetting of initially percolated Au films is yet to be studied. While films displaying large, flat Au islands and a SP band strongly shifted to the IR region are of substantial interest, the scatter in the SP band position has to be further studied.

Critical Au Film Thickness. The transition from films with protruding voids (type I) to partially closed (type II) occurs at a film nominal thickness of ca. 13 nm, i.e., 13 nm films from the same evaporation batch may follow either of the two dewetting scenarios. Figure 1 and Table 1 give two sets of data for 13 nm annealed Au films, corresponding to type I and type II samples. In general, type I islands (<13 nm nominal thickness) are more rounded with a smaller aspect ratio, while type II islands (>13 nm nominal thickness) are oblate with extended flat top surfaces. The average aspect ratio of type II islands reaches ca. 1.4, a value for which splitting of the SP band to transverse and longitudinal components is expected;[72] this issue is further discussed below.

The effect of the critical thickness is demonstrated in Figure 5, where two Au films with similar as-evaporated transmission spectra show a different spectral behavior after annealing, characteristic of type I and type II films.

The data presented in Tables 1 and 2 show that the standard deviations of the characteristic parameters for films with a nominal thickness of 13 nm are higher than those of thinner (12 nm) and thicker (14 nm) films. A possible reason may be lateral inhomogeneity of the unannealed structure on the micrometer scale, such that different parts of the sample after annealing show either type I or type II behavior. We could not identify
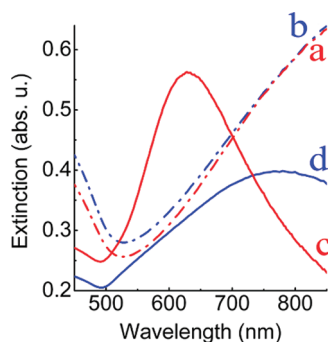
Figure 5. Transmission UV−vis spectra of two 13 nm Au films from the same evaporation batch (traces a and b), revealing type I (trace c) and type II (trace d) spectra following 10 h annealing at 550 °C.

structural or spectral properties of 13 nm as-evaporated films that might predict their classification after annealing, and this is still an open issue.

Absorption and Scattering in Au Island Films. Extinction spectra of Au films measured in the standard near-normal transmission mode in air, as those shown in Figure 2, present a combination of absorption and scattering. To assess their relative contributions and dependence on the film morphology, measurements of the total reflectance (Ref) and transmittance (Tr) were carried out using an integration sphere, allowing separation of the absorption (Abs) and scattering (Sc) components of the extinction (Ext) for the different spectra

$$\text{Abs}(\%) = 100 - \text{Ref}(\%) - \text{Tr}(\%) \quad (1)$$

$$\text{Ext}(\%) = \text{Abs}(\%) + \text{Ref}(\%) \quad (2)$$

Literature reports indicate that for islands with a major axis smaller than ca. 50 nm (i.e., up to ca. 7.5 nm nominal thickness in the present system) the extinction is dominated by the absorbance.[1,65,76] Above this island size the contribution of scattering to the total extinction becomes increasingly important, as seen in the results presented in Figure 6 for type II films. Extinction spectra of islands larger than ca. 200 nm are dominated by scattering (Figure 6D, 6E, 6J, and 6K). These results are in agreement with previously published data for Au nanodisks prepared by colloidal lithography.[65]

Refractive Index Sensitivity (RIS). The bulk refractive index sensitivity (RIS, also denoted m) is defined as the change of spectral parameters of the LSPR transducer in response to change in the refractive index (RI) of the bulk medium. The RIS is one of the two basic parameters (together with the SP decay length, l) defining the sensitivity of an LSPR transducer to binding of an analyte layer.[6,77] In a simple phenomenological model,[77−79] the response (Res) of the transducer to analyte binding is expressed by

$$\text{Res} = m\Delta n[1 - \exp(-d/l)] \quad (3)$$

where m is the RIS of the transducer, Δn is the difference between the RI of the analyte and the medium, l is the effective decay length of the SP electromagnetic field, and d is the effective thickness of the bound analyte layer. The RIS is related to the specific parameter chosen, i.e., wavelength shift, intensity change, band shape, etc. According to eq 3 the value of the bulk RIS represents the maximum response attainable using a given transducer, and is commonly used as a basic parameter for initial
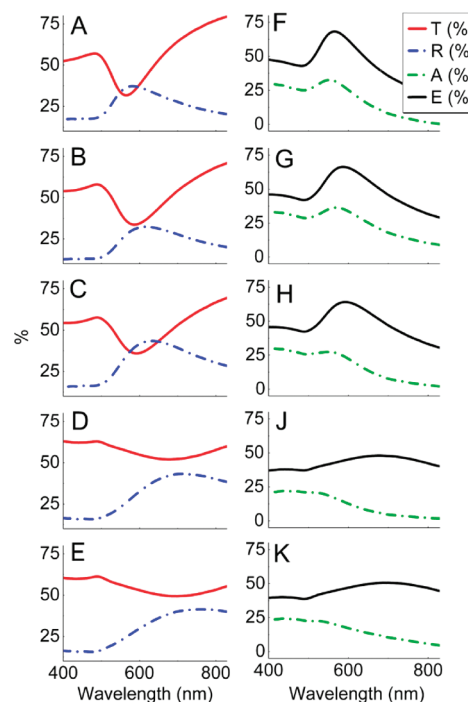

Figure 6. Measured transmission, reflection, and extinction spectra and calculated absorption spectra (using eq 1) for (A, F) 10, (B, G) 11, (C, H) 12, (D, J) 14, and (E, K) 15 nm (nominal thicknesses) Au films evaporated on glass substrates and annealed 10 h at 550 °C (measured in air).

evaluation of the LSPR transducers sensitivity.[2,80] A correlation between the RIS and the SP decay length was demonstrated recently.[77]

We previously reported[3] RIS values of 66−121 nm RIU^{-1} and 0.2−0.54 abs.u. RIU^{-1}, respectively, for wavelength shift, m_λ, and for intensity change, m_{Ext}, of Au island films (2.5, 5.0, and 7.5 nm nominal thickness) evaporated on silanized glass and annealed 20 h at 200 °C, while Au islands evaporated on bare glass and annealed 10 h at 550 or 600 °C showed RIS values of 93−153 nm RIU^{-1} and 0.23−0.81 abs.u. RIU^{-1}. The RIS m_λ exhibited a near-linear dependence on the SP band wavelength, increasing with the red shift of the SP band maximum.[3]

The RIS of Au films studied in the present work (types I and II) was determined using measurements in a series of solvents with varying RI values[3] (Figure 7A and 7B), showing a regular red shift of the SP band with an increase in the RI of the medium, in agreement with the Maxwell−Garnett effective medium theory.[81] The spectral response to RI change is, however, significantly different for type I and II films: While the red shift of the SP band in type I films is accompanied by a corresponding increase in the extinction intensity, the extinction intensity of type II films remains nearly constant. In this respect, type II films display a spectral behavior different from that of all other evaporated−annealed Au island films studied by us.[3,7] The dependence of the SP wavelength on the RI of the bulk medium is presented in more detail in Figure 7C and 7D, showing normalized data. Notably, the red shift of the SP maximum with the medium RI for type II films is exceptionally large, ca. 4 times larger compared to that of type I films.

The RIS m_{Ext} is commonly determined as extinction intensity change at a constant wavelength, usually somewhat red shifted from the SP peak.[6,77,82] An analogous approach can be adopted
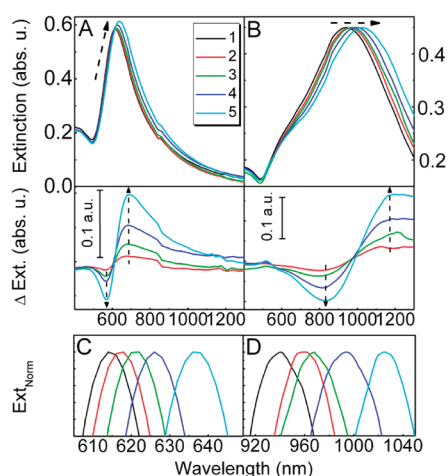
Figure 7. Transmission UV−vis spectra of 10 (A, C) and 15 nm (B, D) Au island films, annealed 10 h at 550 °C, measured in solvents with different refractive index (RI) values. Arrows in A and B (top panels) indicate an increase of the RI of the solution from methanol (1) to ethanol (2), heptane (3), propylene carbonate (4), and toluene (5). Bottom panels in A and B show difference spectra obtained by subtracting the spectrum in methanol from the other spectra; arrows indicate the wavelength values chosen for RIS measurements at a constant wavelength (see text). (C and D) Magnified normalized spectra in A and B, respectively.

for obtaining m_λ, namely, change of the wavelength at a constant (predefined) extinction intensity value, furnishing an easily determined parameter. A line drawn at a constant extinction intersects the spectra twice: in the shorter wavelength (SW) region of the spectrum and in the longer wavelength (LW) region (Figure 7A and 7B), providing a convenient means of determining the wavelength shift. Spectral changes measured in this manner are larger than those obtained by the standard calculations using the shift of the SP band maximum, m_λ^{max}.

Figure 8 depicts RIS calculations based on the spectra in Figure 7 using the following definitions: (a) RIS as wavelength shift at a constant extinction, m_λ^{Ext} (measured at 0.50 abs.u. for type I and at 0.31 abs.u. for type II films); (b) RIS as intensity change at a constant wavelength, in the SW (m_{Ext}^{λ}, 580 nm for type I and 820 nm for type II films) and LW (m_{Ext}^{λ}, 680 nm for type I and 1160 nm for type II films) regions of the spectrum; and (c) the common RIS calculation, as a shift of the maximum SP wavelength (m_λ^{max}) and intensity change at the SP maximum (m_{Ext}^{max}). RIS values calculated according to the above definitions are summarized in Table 3.

The data in Table 3 indicate that RIS values derived at a constant extinction or wavelength are not only more convenient and accurate to measure but also substantially higher than the respective values obtained at the SP band maximum. As expected, m_λ values measured in the SW region of the spectrum are smaller than those calculated in the LW region. Type II Au islands exhibit exceptionally large RIS m_λ, reaching values which are considerably higher than those reported for type I films[3] and other Au island films.[7] Additional experiments are necessary to compare the signal-to-noise ratio in the proposed modes of sensing to known procedures using wavelength shift,[83−85] extinction difference,[3,6,75,86] or centroid.[87,88]

Theoretical calculations (DDA computations and analytical approximations)[5,89] and experimental data[89] have indicated a
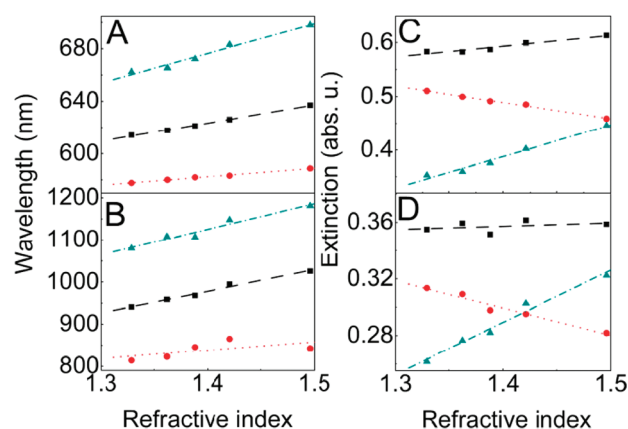

Figure 8. RIS measurements using various definitions, for type I (10 nm) (A, C) and type II (15 nm) (B, D) Au island films, annealed 10 h at 550 °C. (A and B) Wavelength shift vs RI, measured either at the SP band maximum (black squares) or at a constant extinction intensity in the SW (red circles) and LW (green triangles) spectral region (constant extinction values: type I, 0.31 abs.u.; type II, 0.5 abs.u.). (C and D) Extinction intensity change vs RI, measured either at the SP band maximum (black squares) or at a constant wavelength of (C) 580 and (D) 820 nm (red circles) and (C) 680 and (D) 1160 nm (green triangles). RIS values m_λ^{max}, m_λ^{Ext}, m_{Ext}^{max}, and m_{Ext}^{λ} are obtained as the fitted linear regression slopes.

Table 3. Characteristic RIS Values of Type I (10 nm) and Type II (15 nm) Au Films, Annealed 10 h at 550 °C, Measured at the SP Band Maximum (m_λ^{max}, m_{Ext}^{max}) as well as at a Constant Intensity (m_λ^{Ext}) and Constant Wavelength (m_{Ext}^{λ}), at Shorter (SW) and Longer (LW) Wavelengths

nominal film thickness (nm)	10	15
m_λ^{Ext} (nm RIU^{-1}), SW	65	308
m_λ^{Ext} (nm RIU^{-1}), LW	226	613
m_λ^{max} (nm RIU^{-1})	139	516
m_{Ext}^{λ} (abs.u. RIU^{-1}), SW	−0.300	−0.192
m_{Ext}^{λ} (abs.u. RIU^{-1}), LW	0.590	0.369
m_{Ext}^{max} (abs.u. RIU^{-1})	0.200	0.020

generally linear correlation between m_λ and the SP band wavelength for various Au nanostructures. We previously presented a compilation of experimental data supporting this notion.[3] Figure 9 provides a more extensive compilation, including the results of the present work. The combined experimental data are in qualitative agreement with the theoretical calculations, i.e., m_λ increases rather regularly with the wavelength of the SP band maximum. The apparent generality of this correlation implies that m_λ can be roughly estimated from the SP band position.[3]

The performance of the LSPR transducers was evaluated by means of the commonly used dimensionless figure-of-merit (FOM) defined as the ratio between m_λ^{max} and the full width at half-maximum (fwhm) of the SP band.[90,91] (Note that a FOM can be similarly calculated for m_λ^{Ext}; here we chose to use the usual definition.) Values of the FOM for Au transducers studied in the present work are reported in Table 2; these values are substantially higher than those reported for type I films.[3] The results in Tables 2 and 3 show that type II films display high RIS and FOM values, which are larger than those reported for nanosphere lithography fabricated Ag nanoparticles (NPs),[92] Au nanoshells,[93]
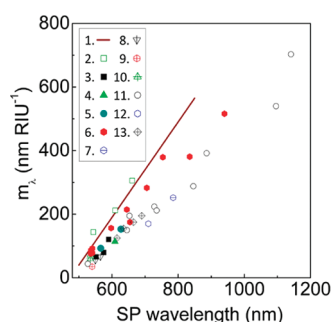
Figure 9. Correlation between the RIS m_λ and the SP band wavelength for a variety of Au nanostructures: (1) theoretical model;[5] (2) numerical DDA calculation;[5] (3) islands on silanized glass, annealed at 200 °C;[75] (4 and 5) islands on bare glass, annealed at 550 and 600 °C, respectively;[64] (6) 2, 3, 4, 5, 10, 11, 12, 13, 14, and 15 nm island films on bare glass, annealed 10 h at 550 °C (present work, given as m_λ^{max}); (7) nanorods;[103] (8) islands partially embedded in silica;[104] (9) NPs on glass;[105] (10) NPs in solution;[106] (11) nanostructures of variable shape in solution;[2] (12) nanorods;[107] (13) nanorods.[108] The SP band wavelength is given in methanol, $n = 1.329$, neglecting the minor effect of the glass substrate (current work), and in water, $n = 1.330$ (literature data).

and of the same order of magnitude as those of Ag nanowells,[90] Au nanohole arrays,[94] nanobipyramides,[2] and nanobranches.[2]

It should be noted that the overall sensitivity of LSPR transducers to specific analytes is determined not only by the RIS but also by the decay length (l) of the SP evanescent field (eq 3). In actual applications both parameters should be tailored to the studied system to obtain maximal transducer response.[77]

Modeling of the Optical Properties. Numerical simulations using the program DDSCAT[68−70] based on the discrete dipole approximation (DDA) were employed in order to model the optical properties of the Au islands. The dielectric function of Au reported by Johnson and Christy[95] was used in the calculation. For convenience, the simulations were carried out for islands in a homogeneous nonabsorbing dielectric medium with a refractive index of $n = 1.500$. The numerical results were compared to experimental data for annealed Au islands partially embedded in a glass substrate ($n = 1.520$) and immersed in toluene ($n = 1.496$), thus providing a nearly homogeneous medium. Normal incidence of the light impinging on the substrate was assumed. Simulated spectra were averaged over the different possible orientations of light polarization with respect to the islands, thus accounting also for the random orientations of the islands within the experimental ensemble. As an approximation of the experimental data, based on our previous reports[3] (Figure S6, Supporting Information), the island shape was modeled as a truncated ellipsoid by introducing facets (insets in Figure 10) and modeled by discretization of the island volume to cubic unit cells of 1 nm³. SP coupling effects were not considered, based on the large average distance between adjacent islands in the annealed films.[96] Typical island dimensions corresponding to films of different nominal thicknesses were extracted from experimental HRSEM and AFM data (see Table S1, Supporting Information). The size distribution of the islands in a given experimental sample was included in the simulations by averaging the spectra of single islands obtained for different dimensions and weighted using the experimental island size distributions (Figure S7, Supporting Information), taking into account the island aspect ratio (AR).[97] An example of such a calculation (for annealed 10 nm Au island sample) is given in the Supporting Information.
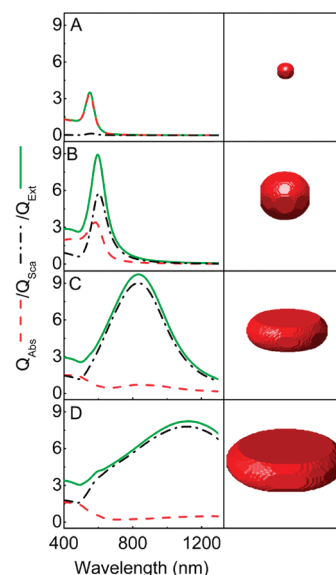

Figure 10. Calculated efficiency of the absorption (Q_{Abs}), scattering (Q_{Sca}), and extinction (Q_{Ext}) for single Au islands embedded in a homogeneous medium ($n = 1.500$). Island dimensions: (A) major axis, 28 nm; AR, 1.11; (B) major axis, 72.4 nm; AR, 1.11; (C) major axis, 131 nm; AR, 1.24; (D) major axis, 191 nm; AR, 1.38. Insets show the island models in correct proportions.

Calculated absorption (Q_{Abs}), scattering (Q_{Sca}), and extinction (Q_{Ext}) efficiencies of single Au islands with increasing dimensions and aspect ratio, embedded in a homogeneous medium with a refractive index of $n = 1.500$, show a systematic red shift of the SP extinction peak as size increases (Figure 10). Mie calculations[98,99] predict that the major component in the extinction of small particles is absorption, while the contribution of scattering is insignificant, as seen in the present results (Figure 10A). In cases where absorption dominates the SP band is narrow with only a small red shift, i.e., the peak is located around 540 nm. Upon island enlargement the contribution of absorption to the extinction spectrum remains approximately constant (Figure 10A and 10B), while the scattering efficiency gradually increases, eventually becoming dominant (Figure 10C and 10D). At the same time the SP band becomes much broader and shifts considerably to longer wavelengths. Hence, the red shift and band broadening are influenced primarily by scattering. The large island with an AR of 1.38 displays two SP peaks, around 600 and 1120 nm (Figure 10D), attributed to different multipoles.[100] Growth of the scattering/absorption ratio with increasing island volume has been related to an increase of the radiative damping in large NPs.[98,101,102]

Spectra (Q_{Ext}) calculated for single islands using several combinations of structural parameters are shown in Figure 11. Splitting of the spectra to longitudinal and transversal SPs is observed for islands with a major axis of 52 nm and both aspect ratios (Figure 11A). These islands are a major component of type I films (Figure S7, Supporting Information). On the other hand, the experimental extinction data show a single SP peak for type I films (Figure 12A). This discrepancy is explained by the size and shape distribution of the islands in the ensemble as well as by their random in-plane orientation on the substrate surface.[72] When the experimental size distribution is included in the calculation (Figures S7, S8, and S9 and eq S1, Supporting Information),
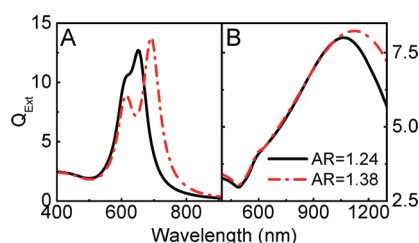
24649

dx.doi.org/10.1021/jp209114j |*J. Phys. Chem. C* 2011, 115, 24642–24652

Figure 11. Calculated spectra (as Q_{Ext}) of single Au islands embedded in a homogeneous medium ($n = 1.500$) with a major axis of 52 (A) and 191 nm (B); AR is 1.24 (black full lines) and 1.38 (red dashed−dotted lines).
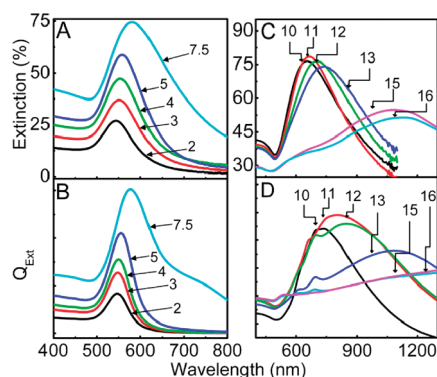

Figure 12. (A and C) Experimental extinction spectra of evaporated Au films, annealed 10 h at 550 °C, measured in toluene ($n = 1.496$). (B and D) Calculated extinction efficiencies of Au island films with a similar island size distribution as in A and B, respectively, embedded in a homogeneous medium ($n = 1.500$). Nominal film thicknesses are indicated.

qualitative agreement between the calculated and the experimental results is obtained (Figure 12A and 12B).

Spectra calculated for single islands with a major axis smaller than 23 nm show a minor red shift of the resonance upon increasing the island size, while the intensity increases considerably. This behavior is predicted by the Mie theory for spheres[98,99] and also holds for islands that are significantly smaller than the wavelength of light. Inserting the actual island size distribution into the calculations (Figures S7, S8, and S9 and eq S1, Supporting Information) leads to a more significant red shift of the extinction spectra with average island size, in qualitative agreement with the experimental data (Figure 12A).

In the case of islands whose sizes are of the same order as the wavelength of the incident light, Figure 11B shows that the difference in optical behavior of islands with different aspect ratios is small. The latter suggests that spectra calculated for single islands (Figures 10 and 11) can be used to describe the experimental spectral features of such films, i.e., splitting and substantial red shift of the SP band, as well as line broadening and decrease of the extinction intensity. The spectral features are attributed to the appearance of quadrupole and octupole peaks, while the dipolar resonance is located in the infrared region (Figure 12D). In this case consideration of island size distribution does not produce better fitting of the experimental data (Figure 12C and 12D).

CONCLUSIONS

Thermal evaporation of gold onto glass substrates followed by annealing in air at a high temperature (≥ 550 °C) is a convenient

scheme for obtaining random island films displaying well-defined localized plasmon properties. In the present work we concentrated on Au films which are initially (i.e., before annealing) near-percolated or just-percolated. Annealing promotes Au dewetting, proceeding via two different mechanisms depending on the film nominal thickness: while unannealed just-percolated Au films ("type I") show a grain morphology with voids that protrude to the glass substrate, in thicker (unannealed) percolated films ("type II") the voids do not reach the glass substrate. This difference in the initial morphology determines the depercolation pathway as well as the structural and optical properties of the resulting films. The structural transformation upon annealing is essentially completed within a few minutes, after which the major process is slow embedding of the Au islands in the glass substrate. The variability in the film initial structure and the different depercolation mechanisms enable tuning of the SP band in a wide wavelength range from the visible to the NIR. With the increase in nominal thickness (and average island size) the optical response shows a transition from absorbance-dominated to scattering-dominated spectra, demonstrated experimentally and theoretically. Numerical simulations were carried out using the DDA approach, taking into account the shape and size distribution in the actual island film samples. The results exhibited satisfactory agreement with the experimental spectra, reproducing the large red shift at increased film nominal thicknesses.

The refractive index sensitivity (RIS) of the studied Au island films shows an intriguing behavior. The annealed type I and type II films both exhibit a near-linear red shift of the SP band maximum in the measured RI range, with type II films displaying particularly high RIS values for wavelength shift. Interestingly, an increase in the RI of the medium produces a significant increase in the maximum extinction intensity of annealed type I films and nearly no change in type II films. On the basis of these results we proposed a simple scheme for maximizing the RIS, i.e., calculation (or measurement) at a constant extinction or at a constant wavelength, with the choice being made on the basis of the specific island transducer used.

The stability, optical response, and simple preparation procedure make the random depercolated Au island system particularly suitable for applications where high RIS values and tunability of the SP band in a wide wavelength range are required.

ASSOCIATED CONTENT

ⓢ Supporting Information. HRSEM images of Au films; temperature profile during annealing; AFM images of Au island footprints in the glass; dispersion of island properties; AFM images of Au islands; size distribution of Au islands; details on the theoretical calculations. This material is available free of charge via the Internet at http://pubs.acs.org.

AUTHOR INFORMATION

Corresponding Author
*Phone: +972-8-9342574 (A.V.); +972-8-9342678 (I.R.). Fax: +972-8-9344137. E-mail: alexander.vaskevich@weizmann.ac.il (A.V.); israel.rubinstein@weizmann.ac.il (I.R.).

ACKNOWLEDGMENT

■ REFERENCES

(1) Kreibig, U.; Vollmer, M. *Optical Properties of Metal Clusters*; Springer: Berlin, 1995.

(2) Chen, H.; Kou, X.; Yang, Z.; Ni, W.; Wang, J. *Langmuir* **2008**, *24*, 5233–5237.

(3) Karakouz, T.; Holder, D.; Goomanovsky, M.; Vaskevich, A.; Rubinstein, I. *Chem. Mater.* **2009**, *21*, 5875–5885.

(4) Lee, K. S.; El-Sayed, M. A. *J. Phys. Chem. B* **2006**, *110*, 19220–19225.

(5) Miller, M. M.; Lazarides, A. A. *J. Phys. Chem. B* **2005**, *109*, 21556–21565.

(6) Nath, N.; Chilkoti, A. *Anal. Chem.* **2004**, *76*, 5370–5378.

(7) Vaskevich, A.; Rubinstein, I. In *Handbook of Biosensors and Biochips*; Marks, R., Cullen, D., Lowe, C., Weetall, H. H., Karube, I., Eds.; Wiley: Chichester, 2007; Vol. 1, pp 447−469.

(8) Willets, K. A.; Van Duyne, R. P. *Annu. Rev. Phys. Chem.* **2007**, *58*, 267–297.

(9) Stewart, M. E.; Anderton, C. R.; Thompson, L. B.; Maria, J.; Gray, S. K.; Rogers, J. A.; Nuzzo, R. G. *Chem. Rev.* **2008**, *108*, 494–521.

(10) Hutter, E.; Fendler, J. H. *Adv. Mater.* **2004**, *16*, 1685–1706.

(11) Anker, J. N.; Hall, W. P.; Lyandres, O.; Shah, N. C.; Zhao, J.; Van Duyne, R. P. *Nat. Mater.* **2008**, *7*, 442–453.

(12) Sannomiya, T.; Hafner, C.; Vörös, J. *J. Biomed. Opt.* **2009**, *14*, 064027–6.

(13) Nusz, G. J.; Marinakos, S. M.; Curry, A. C.; Dahlin, A.; Höök, F.; Wax, A.; Chilkoti, A. *Anal. Chem.* **2008**, *80*, 984–989.

(14) Sannomiya, T.; Scholder, O.; Jefimovs, K.; Hafner, C.; Dahlin, A. B. *Small* **2011**, *7*, 1653–1663.

(15) Svedendahl, M.; Chen, S.; Dmitriev, A.; Käll, M. *Nano Lett.* **2009**, *9*, 4428–4433.

(16) Huang, X.; Jain, P. K.; El-Sayed, I. H.; El-Sayed, M. A. *Nanomedicine* **2007**, *2*, 681–693.

(17) Corrigan, T.; Guo, S.; Phaneuf, R.; Szmacinski, H. *J. Fluoresc.* **2005**, *15*, 777–784.

(18) Biteen, J. S.; Lewis, N. S.; Atwater, H. A.; Mertens, H.; Polman, A. *Appl. Phys. Lett.* **2006**, *88*, 131109–3.

(19) Lee, K.-S.; El-Sayed, M. A. *J. Phys. Chem. B* **2006**, *110*, 19220–19225.

(20) Liz-Marzan, L. M. *Langmuir* **2006**, *22*, 32–41.

(21) Zhang, J. Z.; Noguez, C. *Plasmonics* **2008**, *3*, 127–150.

(22) Noguez, C. *J. Phys. Chem. C* **2007**, *111*, 3806–3819.

(23) Jain, P. K.; Huang, X. H.; El-Sayed, I. H.; El-Sayed, M. A. *Acc. Chem. Res.* **2008**, *41*, 1578–1586.

(24) Murphy, C. J.; Gole, A. M.; Hunyadi, S. E.; Stone, J. W.; Sisco, P. N.; Alkilany, A.; Kinard, B. E.; Hankins, P. *Chem. Commun.* **2008**, 544–557.

(25) Ueno, K.; Juodkazis, S.; Mino, M.; Mizeikis, V.; Misawa, H. *J. Phys. Chem. C* **2007**, *111*, 4180–4184.

(26) Chen, J.; Wiley, B.; Li, Z. Y.; Campbell, D.; Saeki, F.; Cang, H.; Au, L.; Lee, J.; Li, X.; Xia, Y. *Adv. Mater.* **2005**, *17*, 2255–2261.

(27) Skrabalak, S. E.; Chen, J.; Sun, Y.; Lu, X.; Au, L.; Cobley, C. M.; Xia, Y. *Acc. Chem. Res.* **2008**, *41*, 1587–1595.

(28) Xia, Y.; Li, W.; Cobley, C. M.; Chen, J.; Xia, X.; Zhang, Q.; Yang, M.; Cho, E. C.; Brown, P. K. *Acc. Chem. Res.* **2011**, *44*, 914−924.

(29) Hulteen, J., C.; Van Duyne, R., P. *J. Vac. Sci. Technol., A* **1995**, *13*, 1553–1558.

(30) Hanarp, P.; Käll, M.; Sutherland, D. S. *J. Phys. Chem. B* **2003**, *107*, 5768–5772.

(31) Fredriksson, H.; Alaverdyan, Y.; Dmitriev, A.; Langhammer, C.; Sutherland, D. S.; Zäch, M.; Kasemo, B. *Adv. Mater.* **2007**, *19*, 4297–4302.

(32) Fleischer, M.; Zhang, D.; Braun, K.; Jäger, S.; Ehlich, R.; Häffner, M.; Stanciu, C.; Hörber, J. K. H.; Meixner, A. J.; Kern, D. P. *Nanotechnology* **2010**, *21*, 065301.

(33) Baba, K.; Okuno, T.; Miyagi, M. *Appl. Phys. Lett.* **1993**, *62*, 437–439.

(34) Gupta, G.; Tanaka, D.; Ito, Y.; Shibata, D.; Shimojo, M.; Furuya, K.; Mitsui, K.; Kajikawa, K. *Nanotechnology* **2009**, 20.

(35) Gupta, R.; Dyer, M. J.; Weimer, W. A. *J. Appl. Phys.* **2002**, *92*, 5264–5271.

(36) Nakashima, H.; Omoto, H.; Wakabayashi, H. *J. Appl. Phys.* **2004**, *95*, 7790–7797.

(37) Norrman, S.; Andersson, T.; Granqvist, C. G.; Hunderi, O. *Phys. Rev. B* **1978**, *18*, 674–695.

(38) Sennett, R. S.; Scott, G. D. *J. Opt. Soc. Am. A* **1950**, *40*, 203–211.

(39) Szunerits, S.; Praig, V. G.; Manesse, M.; Boukherroub, R. *Nanotechnology* **2008**, *19*, 195712.

(40) Semin, D. J.; Rowlen, K. L. *Anal. Chem.* **1994**, *66*, 4324–4331.

(41) Kaluzhny, G.; Vaskevich, A.; Schneeweiss, M. A.; Rubinstein, I. *Chem.—Eur. J.* **2002**, *8*, 3849–3857.

(42) Doron-Mor, I.; Barkay, Z.; Filip-Granit, N.; Vaskevich, A.; Rubinstein, I. *Chem. Mater.* **2004**, *16*, 3476–3483.

(43) Weimer, W. A.; Dyer, M. J. *Appl. Phys. Lett.* **2001**, *79*, 3164–3166.

(44) Grand, J.; Adam, P. M.; Grimault, A. S.; Vial, A.; De la Chapelle, M. L.; Bijeon, J. L.; Kostcheev, S.; Royer, P. *Plasmonics* **2006**, *1*, 135–140.

(45) Malinsky, M. D.; Lance Kelly, K.; Schatz, G. C.; Van Duyne, R. P. *J. Phys. Chem. B* **2001**, *105*, 2343–2350.

(46) Xu, G.; Tazawa, M.; Jin, P.; Nakao, S. *Appl. Phys. A: Mater. Sci. Process.* **2005**, *80*, 1535–1540.

(47) Kalyuzhny, G.; Vaskevich, A.; Ashkenasy, G.; Shanzer, A.; Rubinstein, I. *J. Phys. Chem. B* **2000**, *104*, 8238–8244.

(48) Cantale, V.; Simeone, F. C.; Gambari, R.; Rampi, M. A. *Sens. Actuators, B: Chem* **2011**, *152*, 206–213.

(49) Zito, R. R.; Bickel, W. S.; Bailey, W. M. *Thin Solid Films* **1984**, *114*, 241–255.

(50) Jiran, E.; Thompson, C. V. *J. Electron. Mater.* **1990**, *19*, 1153–1160.

(51) Golan, Y.; Margulis, L.; Rubinstein, I. *Surf. Sci.* **1992**, *264*, 312–326.

(52) Muller, C. M.; Spolenak, R. *Acta Mater.* **2010**, *58*, 6035–6045.

(53) Alet, P.-J.; Eude, L.; Palacin, S.; Cabarrocas, P. R. i. *Phys. Status Solidi A* **2008**, *205*, 1429–1434.

(54) Feofanov, A.; Ianoul, A.; Kryukov, E.; Maskevich, S.; Vasiliuk, G.; Kivach, L.; Nabiev, I. *Anal. Chem.* **1997**, *69*, 3731–3740.

(55) Saxena, R.; Frederick, M. J.; Ramanath, G.; Gill, W. N.; Plawsky, J. L. *Phys. Rev. B* **2005**, *72*, 115425.

(56) Van Duyne, R. P.; Hulteen, J. C.; Treichel, D. A. *J. Chem. Phys.* **1993**, *99*, 2101–2115.

(57) Aslan, K.; Malyn, S. N.; Zhang, Y. X.; Geddes, C. D. *J. Appl. Phys.* **2008**, *103*, 084307.

(58) Strekal, N.; Maskevich, A.; Maskevich, S.; Jardillier, J. C.; Nabiev, I. *Biopolymers* **2000**, *57*, 325–328.

(59) Suzuki, Y.; Ojima, Y.; Fukui, Y.; Fazyia, H.; Sagisaka, K. *Thin Solid Films* **2007**, *515*, 3073–3078.

(60) Mullins, W. W. *J. Appl. Phys.* **1957**, *28*, 333–339.

(61) Srolovitz, D. J.; Safran, S. A. *J. Appl. Phys.* **1986**, *60*, 255–260.

(62) Srolovitz, D. J.; Safran, S. A. *J. Appl. Phys.* **1986**, *60*, 247–254.

(63) Sadan, H.; Kaplan, W. *J. Mater. Sci.* **2006**, *41*, 5371–5375.

(64) Karakouz, T.; Tesler, A. B.; Bendikov, T. A.; Vaskevich, A.; Rubinstein, I. *Adv. Mater.* **2008**, *20*, 3893–3899.

(65) Langhammer, C.; Kasemo, B.; Zoric, I. *J. Chem. Phys.* **2007**, *126*, 194702–11.

(66) Svedendahl, M.; Chen, S.; Dmitriev, A.; Käll, M. *Nano Lett.* **2009**, *9*, 4428–4433.

(67) Khlebtsov, N. G.; Bogatyrev, V. A.; Melnikov, A. G.; Dykman, L. A.; Khlebtsov, B. N.; Krasnov, Y. M. *J. Quant. Spectrosc. Radiat. Transfer* **2004**, *89*, 133–142.

(68) Draine, B. T.; Flatau, P. J. *J. Opt. Soc. Am. A* **1994**, *11*, 1491–1499.

(69) Draine, B. T.; Flatau, P. J. *User Guide for the Discrete Dipole Approximation Code DDSCAT 7.1*, 2010. http://arXiv.org/abs/1002.1505v1. http://www.astro.princeton.edu/~draine/DDSCAT.html.

(70) Lance Kelly, K.; Coronado, E.; Zhao, L. L.; Schatz, G. C. *J. Phys. Chem. B* **2003**, *107*, 668–677.

(71) Karakouz, T.; Maoz, B. M.; Lando, G.; Vaskevich, A.; Rubinstein, I. *ACS Appl. Mater. Interfaces* **2011**, *3*, 978–987.

(72) Tesler, A. B.; Karakouz, T.; Maoz, B. M.; Feldman, Y.; Vaskevich, A.; Rubinstein, I. Manuscript in preparation.

(73) Thompson, C. V. *Annu. Rev. Mater. Sci.* **1990**, *20*, 245–268.

(74) Prikulis, J.; Hanarp, P.; Olofsson, L.; Sutherland, D.; Käll, M. *Nano Lett.* **2004**, *4*, 1003–1007.

(75) Bendikov, T. A.; Rabinkov, A.; Karakouz, T.; Vaskevich, A.; Rubinstein, I. *Anal. Chem.* **2008**, *80*, 7487–7498.

(76) Bohren, C. F.; Huffman, D. R. *Absorption and Scattering of Light by Small Particles*; John Wiley & Sons, Inc.: New York, 1983.

(77) Kedem, O.; Tesler, A. B.; Vaskevich, A.; Rubinstein, I. *ACS Nano* **2011**, *5*, 748–760.

(78) Jung, L. S.; Campbell, C. T.; Chinowsky, T. M.; Mar, M. N.; Yee, S. S. *Langmuir* **1998**, *14*, 5636–5648.

(79) Malinsky, M. D.; Lance Kelly, K.; Schatz, G. C.; Van Duyne, R. P. *J. Am. Chem. Soc.* **2001**, *123*, 1471–1482.

(80) Yonzon, C. R.; Stuart, D. A.; Zhang, X.; McFarland, A. D.; Haynes, C. L.; Van Duyne, R. P. *Talanta* **2005**, *67*, 438–448.

(81) Garnett, J. C. M. *Philos. Trans. R. Soc. London, Ser. A* **1904**, *203*, 385–420.

(82) Kalyuzhny, G.; Schneeweiss, M. A.; Shanzer, A.; Vaskevich, A.; Rubinstein, I. *J. Am. Chem. Soc.* **2001**, *123*, 3177–3178.

(83) Stuart, D. A.; Haes, A.; McFarland, A. D.; Nie, S.; Van Duyne, R. P. *Proc. SPIE* **2004**, 5327.

(84) Yonzon, C. R.; Van Duyne, R. P. *Materials Research Society Symposium Proceedings*; Materials Research Society: Warrendale, PA, 2005; Vol. 876E, R7.3.1–R7.3.6.

(85) Zhao, J.; Zhang, X.; Yonzon, C. R.; Haes, A.; Van Duyne, R. P. *Nanomedicine* **2006**, *1*, 219–228.

(86) Gluodenis, M.; Manley, C.; Foss, C. A. *Anal. Chem.* **1999**, *71*, 4554–4558.

(87) Dahlin, A. B.; Tegenfeldt, J. O.; Höök, F. *Anal. Chem.* **2006**, *78*, 4416–4423.

(88) Nenninger, G. G.; Piliarik, M.; Homola, J. *Meas. Sci. Technol.* **2002**, *13*, 2038–2046.

(89) Sannomiya, T.; Sahoo, P. K.; Mahcicek, D. I.; Solak, H. H.; Hafner, C.; Grieshaber, D.; Vörös, J. *Small* **2009**, *5*, 1889–1896.

(90) Hicks, E. M.; Zhang, X.; Zou, S.; Lyandres, O.; Spears, K. G.; Schatz, G. C.; Van Duyne, R. P. *J. Phys. Chem. B* **2005**, *109*, 22351–22358.

(91) Sherry, L. J.; Chang, S.-H.; Schatz, G. C.; Van Duyne, R. P.; Wiley, B. J.; Xia, Y. *Nano Lett.* **2005**, *5*, 2034–2038.

(92) McFarland, A. D.; Van Duyne, R. P. *Nano Lett.* **2003**, *3*, 1057–1062.

(93) Jain, P. K.; El-Sayed, M. A. *J. Phys. Chem. C* **2007**, *111*, 17451–17454.

(94) Brolo, A. G.; Gordon, R.; Leathem, B.; Kavanagh, K. L. *Langmuir* **2004**, *20*, 4813–4815.

(95) Johnson, P. B.; Christy, R. W. *Phys. Rev. B* **1972**, *6*, 4370–4379.

(96) Jain, P. K.; Huang, W.; El-Sayed, M. A. *Nano Lett.* **2007**, *7*, 2080–2088.

(97) Sprunken, D. P.; Omi, H.; Furukawa, K.; Nakashima, H.; Sychugov, I.; Kobayashi, Y.; Torimitsu, K. *J. Phys. Chem. C* **2007**, *111*, 14299–14306.

(98) Jain, P. K.; Lee, K. S.; El-Sayed, I. H.; El-Sayed, M. A. *J. Phys. Chem. B* **2006**, *110*, 7238–7248.

(99) Mie, G. *Ann. Phys.* **1908**, *25*, 377–445.

(100) Shuford, K. L.; Ratner, M. A.; Schatz, G. C. *J. Chem. Phys.* **2005**, 123.

(101) Sönnichsen, C.; Franzl, T.; Wilk, T.; von Plessen, G.; Feldmann, J. *New J. Phys.* **2002**, *4*, 93.

(102) Sönnichsen, C.; Franzl, T.; Wilk, T.; von Plessen, G.; Feldmann, J.; Wilson, O.; Mulvaney, P. *Phys. Rev. Lett.* **2002**, *88*, 077402.

(103) Marinakos, S. M.; Chen, S.; Chilkoti, A. *Anal. Chem.* **2007**, *79*, 5278–5283.

(104) Meli, M. V.; Lennox, R. B. *J. Phys. Chem. C* **2007**, *111*, 3658–3664.

(105) Okamoto, T. *Topics Appl. Phys.* **2001**, *81*, 97–123.

(106) Sun, Y.; Xia, Y. *Anal. Chem.* **2002**, *74*, 5297–5305.

(107) Mayer, K. M.; Lee, S.; Liao, H.; Rostro, B. C.; Fuentes, A.; Scully, P. T.; Nehl, C. L.; Hafner, J. H. *ACS Nano* **2008**, *2*, 687–692.

(108) Ni, W.; Chen, H.; Kou, X.; Yeung, M. H.; Wang, J. *J. Phys. Chem. C* **2008**, *112*, 8105–8109.